

Clustering Time Series with Nonlinear Dynamics: A Bayesian Non-Parametric and Particle-Based Approach

Alexander Lin¹ Yingzhuo Zhang¹ Jeremy Heng¹ Stephen A. Allsop²
 Kay M. Tye³ Pierre Jacob¹ Demba Ba¹

¹Harvard University

²MIT, Picower Institute

³Salk Institute for Biological Sciences

Abstract

We propose a statistical framework for clustering multiple time series that exhibit nonlinear dynamics into an a-priori-unknown number of sub-groups that each comprise time series with similar dynamics. Our motivation comes from neuroscience where an important problem is to identify, within a large assembly of neurons, sub-groups that respond similarly to a stimulus or contingency. In the neural setting, conditioned on cluster membership and the parameters governing the dynamics, time series within a cluster are assumed independent and generated according to a nonlinear binomial state-space model. We derive a Metropolis-within-Gibbs algorithm for full Bayesian inference that alternates between sampling of cluster membership and sampling of parameters of interest. The Metropolis step is a PMMH iteration that requires an unbiased, low variance estimate of the likelihood function of a nonlinear state-space model. We leverage recent results on controlled sequential Monte Carlo to estimate likelihood functions more efficiently compared to the bootstrap particle filter. We apply the framework to time series acquired from the prefrontal cortex of mice in an experiment designed to characterize the neural underpinnings of fear.

1 Introduction

In a data set comprising hundreds to thousands of neuronal time series (Brown et al., 2004), the ability to automatically identify sub-groups of time series that respond similarly to an exogenous stimulus or contingency can provide insights into how neural computation is implemented at the level of groups of neurons.

We consider the problem of clustering multiple time series that exhibit nonlinear dynamics into an a-priori-unknown number of sub-groups. Existing model-based approaches for clustering multiple time series rely on a generative model of the time series that is a mixture of linear-Gaussian state-space models, and can be further classified according to whether the number of mixture components is assumed to be known a priori, and according to the choice of inference procedure (MCMC or variational Bayes) (Inoue et al., 2006; Chiappa and Barber, 2007; Nieto-Barajas et al., 2014; Middleton, 2014; Saad and Mansinghka, 2018). In all cases, the linear-Gaussian assumption is crucial: it enables exact evaluation of the likelihood using a Kalman filter and the ability to sample exactly from the state sequences underlying each of the time series. For nonlinear and/or non-Gaussian state-space models, this likelihood cannot be evaluated in closed form and exact sampling is not possible.

We introduce a framework for clustering multiple time series that exhibit nonlinear dynamics into an a-priori-unknown number of clusters, each modeled as a nonlinear state-space model. We derive a Metropolis-within-Gibbs algorithm for inference in a Dirichlet process mixture of state-space models with linear-Gaussian states and binomial observations, a popular model in the analysis of neural spiking activity (Smith and Brown, 2003). The Metropolis step uses PMMH (Andrieu et al., 2010), which requires likelihood estimates with small variance. We use controlled SMC (Heng et al., 2017) to produce such estimates. We apply the framework to the clustering of 33 neural spiking time series acquired from the prefrontal cortex of mice in an experiment designed to characterize the neural underpinnings of fear. The framework produces a

clustering of the neurons into groups that represent various degrees of neuronal signal modulation during a fear paradigm.

2 Nonlinear Time Series Clustering Model

We begin by introducing, under a general framework, the Dirichlet Process nonlinear State-Space Model (DPnSSM) for clustering multiple time series with nonlinear dynamics.

2.1 DPnSSM

Consider a set of observed time series $\mathbf{Y} = \{\mathbf{y}^{(1)}, \dots, \mathbf{y}^{(N)}\}$ in which each $\mathbf{y}^{(n)}$ is a vector of length T . Let $y_t^{(n)} \in \mathbb{R}$ denote the t -th component of $\mathbf{y}^{(n)}$. We assume that each series $\mathbf{y}^{(n)}$ is the output of a state-space model with hidden state vector $\mathbf{x}^{(n)}$. In particular,

$$\begin{aligned} x_1^{(n)} &\sim h(x_1^{(n)}) & (1) \\ x_t^{(n)} | x_{t-1}^{(n)}, \tilde{\boldsymbol{\theta}}^{(n)} &\sim f(x_{t-1}^{(n)}, x_t^{(n)}; \tilde{\boldsymbol{\theta}}^{(n)}), & t > 1 \\ y_t^{(n)} | x_t^{(n)}, \tilde{\boldsymbol{\theta}}^{(n)} &\sim g(x_t^{(n)}, y_t^{(n)}; \tilde{\boldsymbol{\theta}}^{(n)}), & t \geq 1, \end{aligned}$$

where $\tilde{\boldsymbol{\theta}}^{(n)}$ denotes a set of *hidden parameters* for series n , f is some *state transition function*, g is some *state-dependent likelihood*, and h is some *initial prior*.

The latent variables $\tilde{\boldsymbol{\Theta}} = \{\tilde{\boldsymbol{\theta}}^{(1)}, \dots, \tilde{\boldsymbol{\theta}}^{(N)}\}$ form the basis of clustering $\{\mathbf{y}^{(1)}, \dots, \mathbf{y}^{(N)}\}$. However, since the number of clusters is itself a latent variable, we decide to model the $\tilde{\boldsymbol{\theta}}^{(1)}, \dots, \tilde{\boldsymbol{\theta}}^{(N)}$ as coming from a distribution Q sampled from a Dirichlet process with base distribution G and inverse-variance parameter α (Ferguson, 1973). Recall that Q is essentially discrete with probability 1, that is, the number of distinct values within N draws from Q is random. More formally,

$$\begin{aligned} \tilde{\boldsymbol{\theta}}^{(1)}, \dots, \tilde{\boldsymbol{\theta}}^{(N)} &\sim Q & (2) \\ Q &\sim \text{DP}(\alpha G). \end{aligned}$$

The overall objective is to infer the joint distribution of $\tilde{\boldsymbol{\theta}}^{(1)}, \dots, \tilde{\boldsymbol{\theta}}^{(N)} | \mathbf{Y}, \alpha, G$. To tackle this problem, we employ a Gibbs sampling algorithm (Neal, 2000).

The Chinese Restaurant Process (CRP) representation of the Dirichlet process integrates out the intermediary distribution Q in generating samples of $\tilde{\boldsymbol{\theta}}^{(1)}, \dots, \tilde{\boldsymbol{\theta}}^{(N)}$. The CRP allows us to nicely separate the process of assigning a cluster (i.e. table) to each $\mathbf{y}^{(n)}$ from the process of choosing a hidden parameter (i.e. table value) for each cluster. This is very similar to the finite mixture model, but we do not need to choose K , the number of clusters, a priori (Neal, 2000).

Under the CRP, we index the parameters by the cluster index k instead of the observation index n . Let $z^{(n)} \in \{1, \dots, K\}$ denote the cluster identity of series n and let $\boldsymbol{\theta}^{(k)}$ denote the hidden parameters for cluster k . We formally define the model as follows,

$$\begin{aligned} z^{(1)}, \dots, z^{(N)}, K &| \alpha \sim \text{CRP}(\alpha, N) & (3) \\ \boldsymbol{\theta}^{(k)} &| G \sim G \\ x_1^{(n)} &\sim h(x_1^{(n)}) \\ x_t^{(n)} | x_{t-1}^{(n)}, z^{(n)} = k &\sim f(x_{t-1}^{(n)}, x_t^{(n)}; \boldsymbol{\theta}^{(k)}), & t > 1 \\ y_t^{(n)} | x_t^{(n)}, z^{(n)} = k &\sim g(x_t^{(n)}, y_t^{(n)}; \boldsymbol{\theta}^{(k)}), & t \geq 1, \end{aligned}$$

where $k = 1, \dots, K$, $n = 1, \dots, N$. A graphical model representation of the DPnSSM is shown in Figure 1.

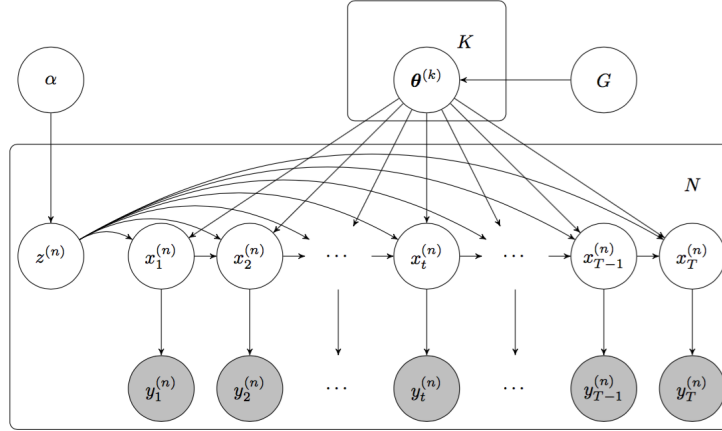


Figure 1: The graphical model representation of the DPnSSM. Observations are shown in grey, and states and parameters are shown in white. For simplicity, we omit the dependencies that are assumed in the DPnSSM between \mathbf{Y} and (Z, Θ) .

2.2 Point Process State-Space Model

While the DPnSSM is defined for generic nonlinear state-space models, in this paper we focus on a state-space model commonly used to model neural spike rasters.

Let $Z = \{z^{(1)}, \dots, z^{(N)}\}$, $\Theta = \{\theta^{(1)}, \dots, \theta^{(K)}\}$. Consider an experiment with R successive trials, during which we record the activity of N neuronal spiking units. Let $(0, T_0]$ be the observation interval for each trial. For each trial r and neuron n , $r = 1, \dots, R$, $n = 1, \dots, N$, let $S_r^{(n)}$ denote the total number of events from the neuronal unit at that trial, and the sequence $0 < \tau_{r,1}^{(n)} < \dots < \tau_{r,S_r^{(n)}}^{(n)}$ correspond to the times at which events from the neuronal unit occur. We assume that $\{\tau_{r,s}^{(n)}\}_{s=1}^{S_r^{(n)}}$ is the realization in $(0, T_0]$ of a stochastic point-process with counting process $N_r^{(n)}(\tau) = \int_0^\tau dN_r^{(n)}(u)$, where $dN_r^{(n)}(\tau)$ is the indicator function in $(0, T_0]$ of $\{\tau_{r,s}^{(n)}\}_{s=1}^{S_r^{(n)}}$. A point-process is fully characterized by its conditional intensity function (CIF) (Vere-Jones, 2003). Assuming trials are independent, the CIF $\lambda^{(n)}(\tau|H_\tau)$ of $dN_r^{(n)}(\tau)$ is defined for all trials as

$$\begin{aligned} \lambda^{(n)}(\tau|H_\tau^{(n)}) & \\ &= \lim_{\Delta \rightarrow 0} \frac{P[N_r^{(n)}(\tau + \Delta) - N_r^{(n)}(\tau) = 1 | H_\tau^{(n)}]}{\Delta}, \end{aligned} \quad (4)$$

where $H_\tau^{(n)}$ is the spiking history of the point process for neuron n up to time τ . The binary discrete-time process obtained by sampling $dN_r^{(n)}(\tau)$ at a resolution of Δ , $T = \lfloor \frac{T_0}{\Delta} \rfloor$, is denoted by $\{\Delta N_{t,r}^{(n)}\}_{t=1,r=1}^{T,R}$. Given constants $x_0^{(n)}, \psi_0$ and assuming independent trials, the following is a popular state-space model (Smith and Brown, 2003) for the discrete-time CIF $\lambda^{(n)}(t)$ of neuron n , $n = 1, \dots, N$,

$$\begin{aligned} x_1^{(n)} &\sim \mathcal{N}(x_0^{(n)}, \psi_0), \\ x_t^{(n)} | x_{t-1}^{(n)} &\sim \mathcal{N}(x_{t-1}^{(n)} + \mu^{(k)} \cdot \mathbb{I}(t = t_0), \psi^{(k)}), & t > 1 \\ \log \frac{\lambda^{(n)}(t)\Delta}{1 - \lambda^{(n)}(t)\Delta} &= x_t^{(n)}, & t > 1 \\ y_t^{(n)} = \sum_{r=1}^R \Delta N_{t,r}^{(n)} &\sim \text{Binomial} \left(R, \frac{e^{x_t^{(n)}}}{1 + e^{x_t^{(n)}}} \right), & t \geq 1. \end{aligned} \quad (5)$$

The state equation in this model imposes a stochastic smoothness constraint on the CIF of neuron n , where $\psi^{(k)}$ controls the degree of smoothness. $\mathbb{I}(t = t_0)$ is an indicator function of the time when the experimenter applies an exogenous stimulus, and is equal to 1 at $t = t_0$, and 0 otherwise. The parameter $\mu^{(k)}$ describes the extent to which the exogenous stimulus modulates the response of the neuron. A positive value of $\mu^{(k)}$ indicates excited neurons, a negative value indicates inhibited neurons, and a value close to zero indicates non-responsive neurons. The parameter $\psi^{(k)}$ describes the variability of the response. A small value of $\psi^{(k)}$ suggests that the neurons exhibit a sustained change in response to the stimulus, whereas a large value of $\psi^{(k)}$ indicates that the change is unsustained.

With respect to the DPnSSM, $\boldsymbol{\theta}^{(k)} = [\mu^{(k)}, \log \psi^{(k)}]^T$. Stated otherwise, the goal is to cluster the neurons according to the extent of their response to the exogenous stimulus $\mu^{(k)}$ and the variability $\psi^{(k)}$ of the response.

3 Inference Algorithm

For conducting posterior inference on the DPnSSM, we introduce a Metropolis-within-Gibbs sampling procedure inspired by Algorithm 8 from Neal (2000). We derive the following process for alternately sampling (1) the cluster assignments $Z \mid \boldsymbol{\Theta}, \mathbf{Y}, \alpha, G$ and (2) the cluster parameters $\boldsymbol{\Theta} \mid Z, \mathbf{Y}, \alpha, G$.

For any set $S = \{s^{(1)}, \dots, s^{(J)}\}$, we use the notation $S^{(-j)} = S \setminus \{s^{(j)}\}$ to denote set S without the j -th element.

3.1 Sampling Cluster Assignments

For a given time series $n \in \{1, \dots, N\}$, we sample its cluster assignment from the distribution:

$$\begin{aligned} p(z^{(n)} \mid Z^{(-n)}, \boldsymbol{\Theta}, \mathbf{Y}, \alpha, G) \\ &\propto p(z^{(n)} \mid Z^{(-n)}, \boldsymbol{\Theta}, \alpha, G) \cdot p(\mathbf{Y} \mid Z, \boldsymbol{\Theta}, \alpha, G) \\ &\propto p(z^{(n)} \mid Z^{(-n)}, \alpha) \cdot p(\mathbf{y}^{(n)} \mid z^{(n)}, \boldsymbol{\Theta}, G). \end{aligned} \quad (6)$$

Due to the CRP's exchangeability property, the first term in Equation (6) can be represented by the categorical distribution

$$p(z^{(n)} = k) = \begin{cases} \frac{N^{(k)}}{N - 1 + \alpha}, & k = 1, \dots, K' \\ \frac{\alpha/m}{N - 1 + \alpha}, & k = K' + 1, \dots, K' + m, \end{cases} \quad (7)$$

where K' is the number of unique k in $Z^{(-n)}$, $N^{(k)}$ is the number of cluster assignments equal to k in $Z^{(-n)}$, and $m \geq 1$ is some integer algorithmic parameter. For brevity, we drop the conditioning on $Z^{(-n)}$ and α .

The second term in Equation (6) is equivalent to the parameter likelihood $p(\mathbf{y}^{(n)} \mid \boldsymbol{\theta}^{(k)})$, where $\boldsymbol{\theta}^{(k)}$ is known if $k \in \{1, \dots, K'\}$; otherwise, $\boldsymbol{\theta}^{(k)}$ must first be sampled from G if $k \in \{K' + 1, \dots, K' + m\}$. In the case of a linear-Gaussian state-space model, Middleton (2014) is able to evaluate this likelihood exactly using a Kalman filter. Since we are modeling $\mathbf{y}^{(n)}$ as the output of a nonlinear state-space model, we must use particle methods to approximate this parameter likelihood. Though the standard bootstrap particle filter (BPF) (Doucet et al., 2001) offers a solution to this problem, it requires many particles to compute a low-variance estimate at the cost of increased computing time. To increase efficiency, we employ a recently proposed method, known as controlled sequential Monte Carlo (cSMC), that significantly reduces the variance of the likelihood estimators for a fixed computational cost (Heng et al., 2017).

3.1.1 Controlled Sequential Monte Carlo

Controlled SMC is based on the idea that we can modify a state-space model in such a way that standard bootstrap particle filters give lower variance estimates while the likelihood of interest is kept unchanged.

More precisely, the algorithm introduces a collection of positive and bounded functions $\gamma = \{\gamma_1, \dots, \gamma_T\}$, termed a policy, that alter the transition probabilities of the model in the following way,

$$h^\gamma(x_1) \propto h(x_1) \cdot \gamma_1(x_1) \quad (8)$$

$$f_t^\gamma(x_{t-1}, x_t; \boldsymbol{\theta}) \propto f(x_{t-1}, x_t; \boldsymbol{\theta}) \cdot \gamma_t(x_t), \quad t > 1. \quad (9)$$

To ensure that the likelihood associated with the modified model is the same as the original one, we introduce a modified version of the state-dependent likelihood g , denoted by $g_1^\gamma, \dots, g_T^\gamma$. On the modified model defined by $h^\gamma, (f_t^\gamma), (g_t^\gamma)$, we can run a standard bootstrap particle filter and compute the likelihood estimator:

$$\hat{p}^\gamma(\mathbf{y} | \boldsymbol{\theta}) = \prod_{t=1}^T \left(\frac{1}{S} \sum_{s=1}^S g_t^\gamma(x_t^s, y_t; \boldsymbol{\theta}) \right), \quad (10)$$

where S is the number of particles and x_t^s is the s -th particle at time t . The policy γ can be chosen so as to minimize the variance of the above likelihood estimator; the optimal policy minimizing that variance is denoted by γ^* .

When h, f are Gaussian and g is log-concave with respect to x_t (such as in the neuroscience application), we can justify the approximation of γ^* with a series of Gaussian functions. This allows us to solve for $h^\gamma, f_2^\gamma, \dots, f_t^\gamma$ and $g_1^\gamma, \dots, g_T^\gamma$ using an approximate backward recursion method that simply reduces to a sequence of linear regressions. We provide a more rigorous treatment of the exact details in the Supplementary Material section.

Starting from an initial policy $\gamma^{(0)}$, we can thus run a first bootstrap particle filter and obtain an approximation $\gamma^{(1)}$ of γ^* . One can then iterate L times to obtain refined policies, and consequently, lower variance estimators of the likelihood. Our empirical testing demonstrates that cSMC can significantly outperform the standard BPF in both precision and efficiency, while keeping L very small. This justifies its use in the DPnSSM inference algorithm.

3.2 Sampling Cluster Parameters

For a given cluster $k \in \{1, \dots, K\}$, we wish to sample from the distribution:

$$\begin{aligned} p(\boldsymbol{\theta}^{(k)} | \boldsymbol{\Theta}^{(-k)}, Z, \mathbf{Y}, \alpha, G) \\ \propto p(\boldsymbol{\theta}^{(k)} | \boldsymbol{\Theta}^{(-k)}, Z, \alpha, G) \cdot p(\mathbf{Y} | \boldsymbol{\Theta}, Z, \alpha, G) \\ \propto p(\boldsymbol{\theta}^{(k)} | G) \cdot \prod_{n | z^{(n)}=k} p(\mathbf{y}^{(n)} | \boldsymbol{\theta}^{(k)}). \end{aligned} \quad (11)$$

The first term of Equation (11) is the prior of the base distribution, and the second term is a product of parameter likelihoods. Because the likelihood conditioned on class membership involves integration of the state sequence $\mathbf{x}^{(n)}$, and the prior G is on the parameters of the state sequence, marginalization destroys any conjugacy that might have existed between the state sequence prior and parameter priors.

To sample from the conditional posterior of parameters given cluster assignments, Middleton (2014) re-introduces the state sequence as part of his sampling algorithm for the linear-Gaussian state-space case. We use an approach that obviates the need to re-introduce the state sequence and generalizes to scenarios where the prior on parameter and the state sequence may not have any conjugacy relationships. In particular, our sampler uses a Metropolis-Hastings step with proposal distribution $r(\boldsymbol{\theta}' | \boldsymbol{\theta})$ to sample from the class conditional distribution of parameters given cluster assignments. This effectively becomes one iteration of the well-known particle marginal Metropolis-Hastings (PMMH) algorithm (Andrieu et al., 2010). To evaluate the second term of Equation (11) for PMMH, we once again choose to use cSMC.

3.3 Full Algorithm

We provide a summary of the full Gibbs Sampling algorithm in Algorithm 1. Outputs are samples $Z^{(i)}, \boldsymbol{\Theta}^{(i)}$ for iterations $i = 1, 2, \dots, I$. Inputs are $\mathbf{Y}, \alpha, G, m, r, I$, along with initial cluster assignments $Z^{(0)}$ and initial cluster parameters $\boldsymbol{\Theta}^{(0)}$.

Algorithm 1 Metropolis-within-Gibbs Inference Procedure for Dirichlet Process Mixture of Nonlinear State-Space Models

```

1: for  $i = 1, \dots, I$  do
2:   Let  $Z = Z^{(i-1)}$  and  $\Theta = \Theta^{(i-1)}$ .
   // Sample cluster assignments.
3:   for  $n = 1, \dots, N$  do
4:     Let  $K'$  be the number of distinct  $k$  in  $Z^{(-n)}$ .
5:     for  $k = 1, \dots, K' + m$  do
6:       Run cSMC to compute  $p(\mathbf{y}^{(n)} \mid \boldsymbol{\theta}^{(k)})$ .
7:     end for
8:     Sample  $z^{(n)} \mid Z^{(-n)}, \Theta, \mathbf{Y}, \alpha, G$ .
9:   end for
10:  Let  $K$  be the number of distinct  $k$  in  $Z$ .
   // Sample cluster parameters.
11:  for  $k = 1, \dots, K$  do
12:    Sample proposal  $\boldsymbol{\theta}' \sim r(\boldsymbol{\theta}' \mid \boldsymbol{\theta}^{(k)})$ .
13:    Run cSMC to compute  $p(\mathbf{y}^{(n)} \mid \boldsymbol{\theta}')$ .
14:    Let  $a = \frac{p(\boldsymbol{\theta}' \mid \Theta^{(-k)}, Z, \mathbf{Y}, \alpha, G) \cdot r(\boldsymbol{\theta}^{(k)} \mid \boldsymbol{\theta}')}{p(\boldsymbol{\theta}^{(k)} \mid \Theta^{(-k)}, Z, \mathbf{Y}, \alpha, G) \cdot r(\boldsymbol{\theta}' \mid \boldsymbol{\theta}^{(k)})}$ .
15:    Let  $\boldsymbol{\theta}^{(k)} = \boldsymbol{\theta}'$  with probability  $\min(a, 1)$ .
16:  end for
17:  Let  $Z^{(i)} = Z$  and  $\Theta^{(i)} = \Theta$ .
18: end for

```

4 Results

We investigate the efficacy of the DPnSSM model in clustering time series obtained from real and simulated neural spike rasters.

4.1 Selecting Clusters

The output of Algorithm 1 is a set of Gibbs samples $(Z^{(1)}, \Theta^{(1)}), \dots, (Z^{(I)}, \Theta^{(I)})$. Each sample $(Z^{(i)}, \Theta^{(i)})$ may very well use a different number of clusters. The natural question that remains is how to select a clustering of our data from this output. There is a great deal of literature on answering this subjective question. We choose to follow the work of Dahl (2006) and Nieto-Barajas et al. (2014).

Each Gibbs sample describes a clustering of the time series; we therefore frame the objective as selecting the most representative sample from our output. To start, we take each Gibbs sample i and construct an $N \times N$ co-occurrence matrix $\Omega^{(i)}$ in which

$$\Omega_{(n,n')}^{(i)} = \begin{cases} 1, & z^{(n)} = z^{(n')} \mid \{z^{(n)}, z^{(n')}\} \in Z^{(i)} \\ 0, & z^{(n)} \neq z^{(n')} \mid \{z^{(n)}, z^{(n')}\} \in Z^{(i)}. \end{cases} \quad (12)$$

This is simply a matrix in which the (n, n') entry is 1 if series n and series n' are in the same cluster for the i -th Gibbs sample and 0 otherwise. We then define $\Omega = (I - B)^{-1} \sum_{i=B+1}^I \Omega^{(i)}$ as the mean co-occurrence matrix, where $B \geq 1$ is the number of pre-burn-in samples. This matrix summarizes information from the entire trace of Gibbs samples. The sample i^* that we ultimately select is the one that minimizes the Frobenius distance to this matrix, i.e.

$$i^* = \arg \min_i \left\| \Omega^{(i)} - \Omega \right\|_F. \quad (13)$$

We use the corresponding assignments $Z^{(i^*)}$ and parameters $\Theta^{(i^*)}$ as the selected clustering. The appeal of this procedure is that it makes use of global information from all the Gibbs samples, yet ultimately selects a single clustering produced by the model.

4.2 Simulated Neural Spiking Data

4.2.1 Data Generation

We simulate $N = 24$ rasters of length $T = 200$ milliseconds exhibiting different responses to an external stimulus applied at $t = 51$ milliseconds. The resolution of the data is $\Delta = 1$ millisecond. Each series $\mathbf{y}^{(n)} = \{y_1^{(n)}, \dots, y_T^{(n)}\}$ comprises points $y_t^{(n)} \in \{0, 1, \dots, 45\}$ that represent the number of times that neuron n fired over $R = 45$ trials at time t . We generat 8 series each of the following three types: (a) *excited* neurons with firing rate λ_1 from $t = \{1, \dots, 50\}$ and a different firing rate λ_2 from $t = \{51, \dots, 200\}$, where $\lambda_1 \sim \text{Uniform}(100, 300)$ Hz and $\lambda_2 \sim \text{Uniform}(700, 900)$ Hz; (b) *inhibited* neurons with firing rate λ_1 from $t = \{1, \dots, 50\}$ and a different firing rate λ_2 from $t = \{51, \dots, 200\}$, where $\lambda_1 \sim \text{Uniform}(700, 900)$ Hz and $\lambda_2 \sim \text{Uniform}(100, 300)$ Hz; and (c) *non-responsive* neurons with firing rate λ for all $t = \{1, \dots, 200\}$, where $\lambda \sim \text{Uniform}(400, 600)$ Hz.

4.2.2 Modeling

In modeling these simulated data, we consider, for simplicity, the case when the cluster parameters is $\theta^{(k)} = \mu^{(k)}$ and each series $y^{(n)}$ is assumed to have been generated by the process

$$\begin{aligned} x_1^{(n)} &\sim \mathcal{N}(x_0^{(n)}, \psi_0) \\ x_t^{(n)} | x_{t-1}^{(n)} &\sim \mathcal{N}(x_{t-1}^{(n)} + \mu^{(k)} \cdot \mathbb{I}(t = 51), \psi), & t > 1 \\ y_t^{(n)} | x_t^{(n)} &\sim \text{Binomial}(45, \sigma(x_t^{(n)})), & t \geq 1, \end{aligned} \tag{14}$$

where $\sigma(x) = (1 + \exp(-x))^{-1}$ is the sigmoid function.

The series are fed into the DPnSSM inference algorithm with hyperparameters $\alpha = 0.1$, $G = \mathcal{N}(0, 1)$, and $m = 5$. For every series n , we compute the initial state $x_0^{(n)} = \sigma^{-1}(1/10 \cdot \sum_{t=1}^{10} y_t^{(n)})$ from the first few observations in that series. In addition, we let $\psi_0, \psi = 10^{-10}$. These are intentionally set to be very small numbers, so any change in effects before $t = 51$ and after $t = 51$ would have to be explained by the cluster parameter $\mu^{(k)}$. For the proposal $r(\mu' | \mu)$, we use a $\mathcal{N}(\mu, 1)$ distribution. We run the Metropolis-within-Gibbs sampling procedure for $I = 500$ iterations and apply a burn-in of $B = 50$ samples. To compute likelihood estimates, we use $L = 4$ cSMC iterations and $S = 64$ particles.

A heatmap of the resultant mean co-occurrence matrix Ω (Equation (12)) can be found in Figure 2. The rows of this matrix are reordered using a dendrogram-based procedure described by Nieto-Barajas et al. (2014). We can observe three distinct clusters that emerge from this visualization. Table 1 summarizes the clustering induced by the chosen Gibbs sample i^* (Equation (13)). It can be seen that the highly positive parameter corresponds to excited neurons, the highly negative parameter corresponds to inhibited neurons, and the near-zero parameter corresponds to non-responsive neurons. The three clusters exactly match the three types of neurons among the 24 rasters, thereby demonstrating the utility of the DPnSSM model.

Table 1: Clustering results for simulation.

$\mu^{(k)}$	$N^{(k)}$	Effect
2.57	8	Excited
-2.82	8	Inhibited
0.10	8	Non-responsive

4.3 Real Neural Spiking Data

In addition to simulations, we produce clusterings on real-world neural spiking data collected in a fear-conditioning experiment in mice designed to elucidate the nature of neural circuits that facilitate the associative learning of fear. The detailed experimental paradigm is described in Allsop et al. (2018). In short, an observer mouse observes a demonstrator mouse receive conditioned cue-shock pairings through a perforated transparent divider. The experiment consists of 45 trials. During the first 15 trials of the experiment, both the observer and the demonstrator simply hear an auditory cue. From trial 16 and onward, the auditory cue

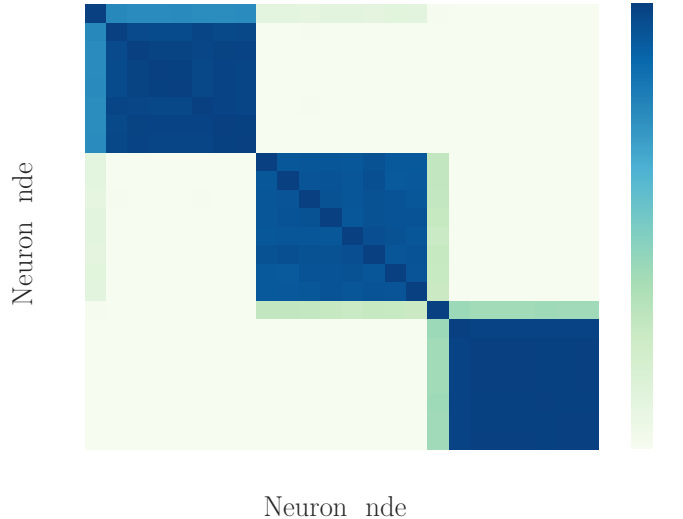


Figure 2: Heatmap of mean co-occurrence matrix for simulation results. The x and y-axis represent neuron indices that are reordered according to the dendrogram-based procedure referred to in the text.

is followed by the delivery of a shock to the demonstrator. The data are recorded from anterior cingulate cortex and basolateral amygdala in the prefrontal cortex of the observer mouse.

We apply DPnSSM to identify various groups of responses in reaction to the auditory cue and the electric shock. A group of neurons that respond significantly to shock can be interpreted as one that allows and observer to understand when the demonstrator is in distress.

4.3.1 Clustering Cue Responses

We analyze data from 33 neurons that are part of a network involved in the associative learning of fear (Allsop et al., 2018). To cluster neurons by their cue responses, we collapse the raster for all neurons over the 45 trials. Thus, for neuron n , each $y_t^{(n)} \in \{0, 1, \dots, 45\}$ represents the number of firings at time t , where $t = 1, \dots, 2000$ milliseconds. The auditory cue is delivered at $t = 501$. We use the following model, which is very similar to that from the simulation:

$$\begin{aligned}
 x_1^{(n)} &\sim \mathcal{N}(x_0^{(n)}, \psi_0) & (15) \\
 x_t^{(n)} | x_{t-1}^{(n)} &\sim \mathcal{N}(x_{t-1}^{(n)} + \mu^{(k)} \cdot \mathbb{I}(t = 501), \psi^{(k)}), & t > 1 \\
 y_t^{(n)} | x_t^{(n)} &\sim \text{Binomial}(45, \sigma(x_t^{(n)})), & t \geq 1,
 \end{aligned}$$

where the cluster parameters are $\theta^{(k)} = [\mu^{(k)}, \log \psi^{(k)}]^T$.

We use $\alpha = 10$, $\mu^{(k)} \sim \mathcal{N}(0, 1)$, $\log \psi^{(k)} \sim \text{Uniform}[-25, 0]$, and $m = 5$. To compute $x_0^{(n)}$, we use an initial period of 500 milliseconds before the start of the time series at $t = 1$, and let $x_0^{(n)} = \sigma^{-1}(p_0^{(n)})$, where $p_0^{(n)}$ is the empirical probability of firing in the initial period. Again, we let $\psi_0, \psi = 10^{-10}$. For the proposal, we let $r(\theta' | \theta^{(k)}) = \mathcal{N}\left(\theta^{(k)}, \begin{bmatrix} 0.01 & 0 \\ 0 & 1 \end{bmatrix}\right)$. To initialize the clustering, we start with all series in a single cluster with parameter $\theta \sim \mathcal{G}$. We run the Metropolis-within-Gibbs sampling for 500 iterations with a burn-in of 50. In calculating parameter likelihoods, we set the maximum number of cSMC iterations to be $L = 4$ and use $S = 64$ particles.

A heatmap of Ω can be found in Figure 3. Table 2 summarizes the chosen clustering. Figure 4 shows two of the nine clusters identified by the algorithm, the highly excited and unsustainable cluster (Figure 4 (a)) and the moderately inhibited and unsustainable cluster (Figure 4 (b)), both with unsustainable responses.

Each of the figures was obtained by overlaying the rasters from neurons in the corresponding cluster. The fact that the overlaid rasters resemble the raster from a single unit (as opposed to random noise) indicates that the algorithm has identified a sensible clustering of the neurons. Figures for all other clusters can be found in the Supplementary Material section.

The algorithm is able to successfully differentiate various types of responses to the cue as well as the variability of the responses. One advantage of not restricting the algorithm to a set number of classes a priori is that it can decide what number of classes best characterizes these data. In this case, the DPnSSM inference algorithm identifies nine different clusters. We defer a scientific interpretation of this phenomenon to a later study.

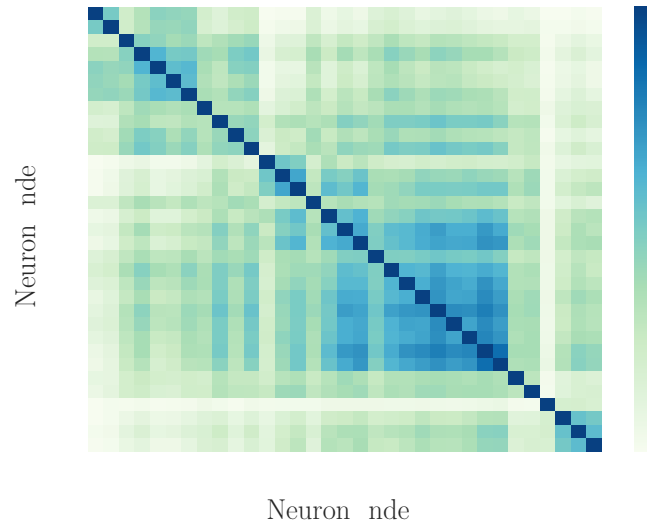


Figure 3: Heatmap of mean co-occurrence matrix for cue response data.

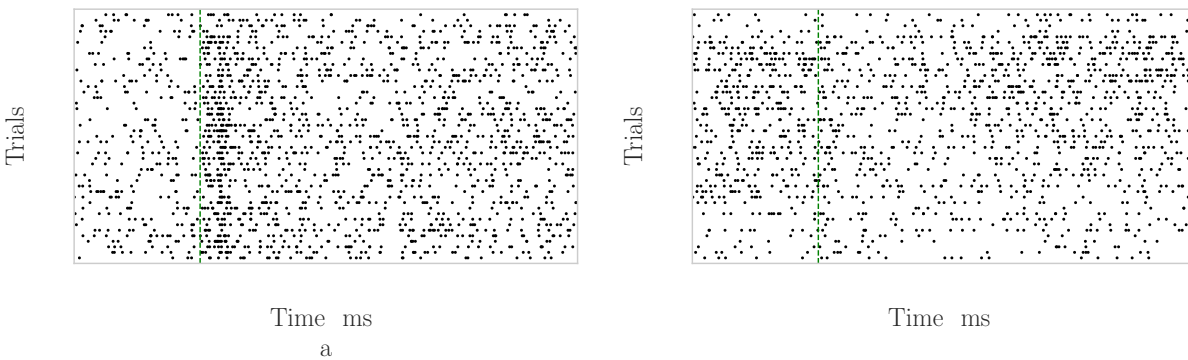


Figure 4: Overlaid raster plots of neurons with (a) highly excited and unsustained responses to the cue, and (b) slightly inhibited and unsustained responses. A black dot indicates a spike from at least one of the neurons in the corresponding cluster. The vertical green indicates cue onset.

Table 2: Clustering results for cue response data analysis.

$\mu^{(k)}$	$\log \psi^{(k)}$	$N^{(k)}$	Effect
0.83	-6.33	4	Highly excited, unsustained
0.55	-7.84	10	Very excited, unsustained
0.45	-10.65	3	Very excited, unsustained
0.33	-15.97	1	Moderately excited, sustained
0.28	-9.59	2	Moderately excited, unsustained
0.16	-22.82	1	Slightly excited, sustained
-0.12	-19.49	2	Slightly inhibited, sustained
-0.18	-8.34	3	Slightly inhibited, unsustained
-0.54	-7.96	7	Very inhibited, unsustained

4.3.2 Clustering Shock Responses

We also apply DPnSSM to determine if neurons can be classified according to varying degrees of neuronal signal modulation when shock is delivered to another animal, as opposed to when there is no shock delivered. The shock is administered starting at the 16-th trial over the 45 trials. Thus, to understand the varying levels of shock effect, we collapse the raster over the 2000 time points. In this setting, each $y_t^{(n)} \in \{0, 1, \dots, 2000\}$ represents the number of firings during the t -th trial. The model is re-formulated as

$$\begin{aligned}
 x_1^{(n)} &\sim \mathcal{N}(x_0^{(n)}, \psi_0) & (16) \\
 x_t^{(n)} | x_{t-1}^{(n)} &\sim \mathcal{N}(x_{t-1}^{(n)} + \mu^{(k)} \cdot \mathbb{I}(t = 16), \psi^{(k)}), & t > 1 \\
 y_t^{(n)} | x_t^{(n)} &\sim \text{Binomial}(2000, \sigma(x_t^{(n)})), & t \geq 1,
 \end{aligned}$$

where the cluster parameters are again $\theta^{(k)} = [\mu^{(k)}, \log \psi^{(k)}]^T$.

For the Dirichlet Process, we use $\alpha = 0.1$, $\mu^{(k)} \sim \mathcal{N}(0, 1)$, $\log \psi^{(k)} \sim \text{Uniform}[-25, -9]$, and $m = 5$. To compute $x_0^{(n)}$, we use data from the first eight trials to first compute $p_0^{(n)} = 1/(8 \cdot 2000) \sum_{t=1}^8 y_t^{(n)}$, and let $x_0^{(n)} = \sigma^{-1}(p_0^{(n)})$. Again, we let $\psi_0, \psi = 10^{-10}$. For the proposal, we let $r(\theta' | \theta^{(k)}) = \mathcal{N}\left(\theta^{(k)}, \begin{bmatrix} 0.01 & 0 \\ 0 & 1 \end{bmatrix}\right)$. To initialize the clustering, we start with all series in a single cluster with parameter $\theta \sim G$. We run the Gibbs sampler for 500 iterations with a burn-in of 50.

The corresponding heatmap, representative raster plots, and clustering results can be found in Figures 5, 6, and Table 3, respectively. We speculate that the results suggest the existence of what we term “*empathy clusters*,” namely groups of neurons that allow an observer to understand when the demonstrator is in distress. We will explore the implications of these findings to the neuroscience of associative learning of fear in future work. The fact that Figure 6(b) comprises neurons that are inhibited is not as visually apparent. In the Supplementary Material Section, we pick two neurons from the cluster and demonstrate that the shock has an inhibitory, albeit subtle, effect on their response.

Table 3: Clustering results for shock response data.

$\mu^{(k)}$	$\log \psi^{(k)}$	$N^{(k)}$	Effect
2.01	-14.8	3.0	Highly excited, unsustained
0.93	-23.22	1.0	Very excited, sustained
0.5	-9.02	5.0	Very excited, unsustained
0.2	-9.36	5.0	Slightly excited, unsustained
-0.1	-21.67	7.0	Slightly inhibited, sustained
-0.33	-9.01	10.0	Moderately inhibited, unsustained
-0.35	-12.23	1.0	Moderately inhibited, unsustained
-1.57	-18.38	1.0	Highly inhibited, unsustained

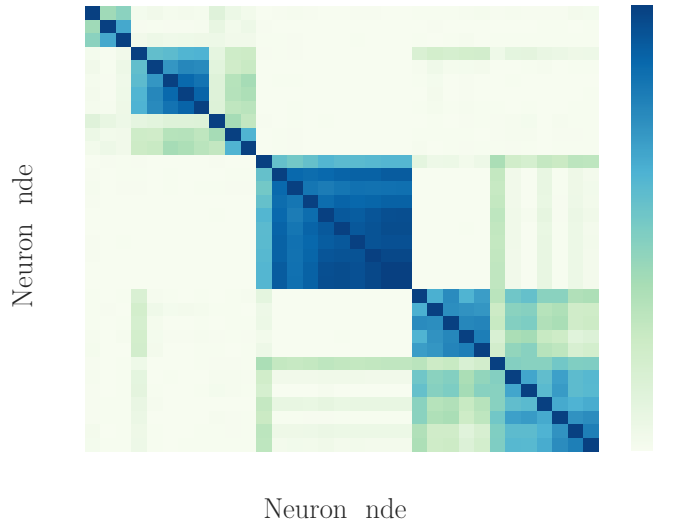


Figure 5: Heatmap of mean co-occurrence matrix for shock response data.

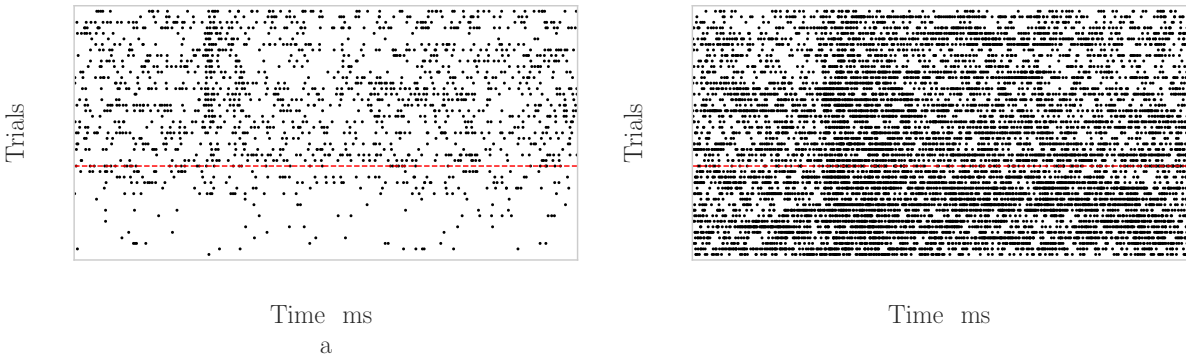


Figure 6: (a) Overlaid raster plots of neurons with (a) highly excited and unsustained responses to the shock, and (b) moderately inhibited and unsustained responses. The horizontal red line indicates the administering of the shock.

4.4 Controlled SMC Versus BPF

Finally, we present some computational results on the advantages of using cSMC over the basic BPF. Computing the parameter likelihood is a fundamental task in Algorithm 1. In each Gibbs iteration, we perform $O(N \cdot K)$ particle filter computations during the sampling of the cluster assignments and another $O(K)$ particle filter computations during the sampling of the cluster parameters. Thus, for both the efficiency and precision of the algorithm, it was necessary to find a fast way to compute low-variance estimates.

From Figure 7, we can observe clear computational benefits of using cSMC. With a mere 64 particles, cSMC can achieve an estimate for the log-likelihood that is lower in variance by an order of magnitude than that of the BPF with 1024 particles. Taking the cost into account, we find that the cSMC algorithm is three times more efficient than the BPF in this example.

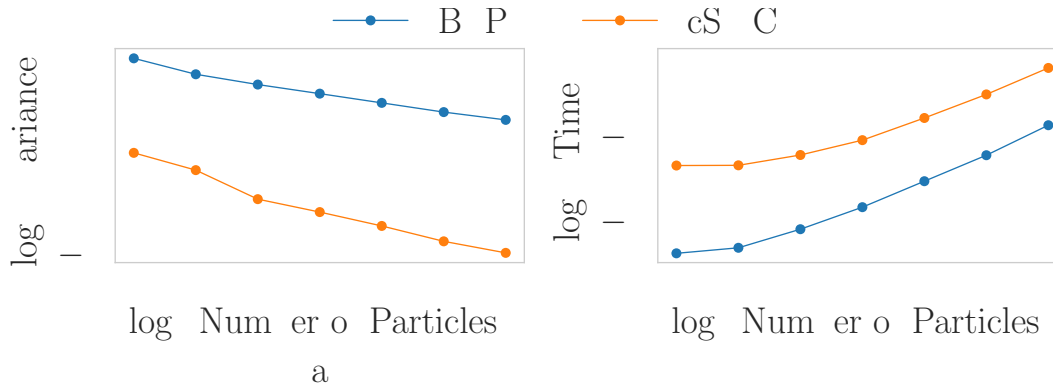


Figure 7: Results on running cSMC and BPF on computing the log parameter likelihood for a representative neuron’s raster plot collapsed across trials. (a) Variance of the log of the likelihood estimate as a function of the number of particles. (b) Computation time in seconds as a function of the number of particles.

5 CONCLUSION

We proposed a general framework to cluster time series with nonlinear dynamics modeled by nonlinear state-space models. To our knowledge, ours is the first Bayesian framework for clustering time series that exhibit nonlinear dynamics. The backbone of the framework is the cSMC algorithm for unbiased, low-variance evaluation of likelihood in nonlinear state-space models. We applied the framework to data recorded from 33 neurons in an experiment designed to elucidate the neural underpinnings of the associative learning of fear in mice, in which one mouse observes another mouse while the latter receives an electric shock. We were able to identify clusters of neurons that allow an observer to understand when the demonstrator is in distress.

In future work, we plan to perform detailed analyses of the data from these experiments (Allsop et al., 2018), and the implications of these analyses on the neuroscience of the associative learning of fear in mice. We will also explore applications of our model to data in other application domains such as sports and sleep research (St Hilaire et al., 2017), to name a few.

References

- Stephen A Allsop, Romy Wichmann, Fergil Mills, Anthony Burgos-Robles, Chia-Jung Chang, Ada C Felix-Ortiz, Alienor Vienne, Anna Beyeler, Ehsan M Izadmehr, Gordon Glober, et al. Corticoamygdala Transfer of Socially Derived Information Gates Observational Learning *Cell*, 173(6):1329–1342, 2018.
- Christophe Andrieu, Arnaud Doucet, and Roman Holenstein. Particle Markov chain Monte Carlo methods. *Journal of the Royal Statistical Society: Series B (Statistical Methodology)*, 72(3):269–342, 2010.
- Emery N Brown, Robert E Kass, and Partha P Mitra. Multiple neural spike train data analysis: state-of-the-art and future challenges. *Nature neuroscience*, 7(5):456, 2004.
- Silvia Chiappa and David Barber. Output Grouping using Dirichlet Mixtures of Linear Gaussian State-Space Models. In *Image and Signal Processing and Analysis, 2007. ISPA 2007. 5th International Symposium on*, pages 446–451. IEEE, 2007.
- David B Dahl. Model-based clustering for expression data via a Dirichlet process mixture model. *Bayesian inference for gene expression and proteomics*, 201:218, 2006.
- Arnaud Doucet, Nando De Freitas, and Neil Gordon. An introduction to sequential Monte Carlo methods. In *Sequential Monte Carlo methods in practice*, pages 3–14. Springer, 2001.

- Thomas S Ferguson. A Bayesian analysis of some nonparametric problems. *The annals of statistics*, pages 209–230, 1973.
- Jeremy Heng, Adrian N Bishop, George Deligiannidis, and Arnaud Doucet. Controlled Sequential Monte Carlo. *arXiv preprint arXiv:1708.08396*, 2017.
- Lurdes YT Inoue, Mauricio Neira, Colleen Nelson, Martin Gleave, and Ruth Etzioni. Cluster-based network model for time-course gene expression data. *Biostatistics*, 8(3):507–525, 2006.
- Lawrence Middleton. Clustering time series: a Dirichlet process mixture of linear-Gaussian state-space models. Master’s thesis, Oxford University, United Kingdom, 2014.
- Radford M Neal. Markov chain sampling methods for Dirichlet process mixture models. *Journal of computational and graphical statistics*, 9(2):249–265, 2000.
- Luis E Nieto-Barajas, Alberto Contreras-Cristán, et al. A Bayesian nonparametric approach for time series clustering. *Bayesian Analysis*, 9(1):147–170, 2014.
- Feras Saad and Vikash Mansinghka. Temporally-Reweighted Chinese Restaurant Process Mixtures for Clustering, Imputing, and Forecasting Multivariate Time Series In *International Conference on Artificial Intelligence and Statistics*, pages 755–764, 2018.
- Anne C Smith and Emery N Brown. Estimating a State-Space Model from Point Process Observations. *Neural computation*, 15(5):965–991, 2003.
- Melissa A St Hilaire, Melanie Rüger, Federico Fratelli, Joseph T Hull, Andrew JK Phillips, and Steven W Lockley. Modeling Neurocognitive Decline and Recovery During Repeated Cycles of Extended Sleep and Chronic Sleep Deficiency *Sleep*, 40(1), 2017.
- David Vere-Jones. *An Introduction to the Theory of Point Processes: Volume I: Elementary Theory and Methods*. Springer, 2003.

Clustering Time Series with Nonlinear Dynamics: A Bayesian Non-Parametric and Particle-Based Approach

Supplementary Material

1 Controlled Sequential Monte Carlo

A key step in sampling both the cluster assignments and the hidden parameters is computing the parameter likelihood $p(\mathbf{y} | \boldsymbol{\theta})$ for an observation vector $\mathbf{y} = \{y_1, \dots, y_T\}$ and a given set of parameters $\boldsymbol{\theta}$.

Recall the state-space model formulation.

$$\begin{aligned} x_1 &\sim h(x_1) \\ x_t | x_{t-1}, \boldsymbol{\theta} &\sim f(x_{t-1}, x_t; \boldsymbol{\theta}) && \text{for all } t = 2, \dots, T \\ y_t | x_t, \boldsymbol{\theta} &\sim g(x_t, y_t; \boldsymbol{\theta}) && \text{for all } t = 1, \dots, T \end{aligned}$$

1.1 Bootstrap Particle Filter

The Bootstrap Particle Filter (BPF) is based on a sequential importance sampling procedure that iteratively approximates each filtering distribution $p(x_t | y_1, \dots, y_t, \boldsymbol{\theta})$ with a set of S particles $\{x_t^1, \dots, x_t^S\}$ so that

$$\hat{p}(\mathbf{y} | \boldsymbol{\theta}) = \prod_{t=1}^T \left(\frac{1}{S} \sum_{s=1}^S g(x_t^s, y_t; \boldsymbol{\theta}) \right)$$

is an unbiased estimate of the parameter likelihood $p(\mathbf{y} | \boldsymbol{\theta})$. We provide a review of this algorithm in Algorithm 2.

Algorithm 2 BootstrapParticleFilter($\mathbf{y}, \boldsymbol{\theta}, f, g, h$)

```

for  $s = 1, \dots, S$  do
  Sample  $x_1^s \sim h(x_1)$ .
  Weight  $w_1^s = g(x_1^s, y_1; \boldsymbol{\theta})$ .
end for
Normalize  $\{w_1^s\}_{s=1}^S = \{w_1^s\}_{s=1}^S / \sum_{s=1}^S w_1^s$ .
for  $t = 2, \dots, T$  do
  for  $s = 1, \dots, S$  do
    Resample ancestor index  $a \sim \text{Categorical}(w_{t-1}^1, \dots, w_{t-1}^S)$ .
    Sample  $x_t^s \sim f(x_{t-1}^a, x_t; \boldsymbol{\theta})$ .
    Weight  $w_t^s = g(x_t^s, y_t; \boldsymbol{\theta})$ .
  end for
  Normalize  $\{w_t^s\}_{s=1}^S = \{w_t^s\}_{s=1}^S / \sum_{s=1}^S w_t^s$ .
end for
return Particles  $\{\{x_1^s\}_{s=1}^S, \dots, \{x_T^s\}_{s=1}^S\}$ 

```

The problem with the Bootstrap Particle Filter (BPF) is that although its estimate of $p(\mathbf{y} | \boldsymbol{\theta})$ is unbiased, this approximation may have high variance for certain observation vectors \mathbf{y} . This variance can be reduced

at the price of increasing the number of particles, yet such a solution significantly increases computation time and is therefore unsatisfactory. To remedy our problem, we follow the work of Heng et al. (2017) in using controlled sequential Monte Carlo (cSMC) as an alternative to the standard particle filter.

1.2 Twisted Sequential Monte Carlo

The basic idea of cSMC is to run several iterations of twisted sequential Monte Carlo, a process in which we redefine the model's state transition function f , initial prior h , and state-dependent likelihood g in a way that allows the BPF to produce lower-variance estimates without changing the parameter likelihood $p(\mathbf{y} | \boldsymbol{\theta})$. See also Guarniero et al. (2017) for a different iterative approach. Using a *policy* $\gamma = \{\gamma_1, \dots, \gamma_T\}$ in which each γ_t is a positive and bounded function, we define

$$\begin{aligned} h^\gamma(x_1) &:= \frac{h(x_1) \cdot \gamma_1(x_1)}{H^\gamma} \\ f_t^\gamma(x_{t-1}, x_t; \boldsymbol{\theta}) &:= \frac{f(x_{t-1}, x_t; \boldsymbol{\theta}) \cdot \gamma_t(x_t)}{F_t^\gamma(x_{t-1}; \boldsymbol{\theta})} \quad \text{for all } t = 2, \dots, T \end{aligned}$$

where $H^\gamma := \int h(x_1) \gamma_1(x_1) dx_1$ and $F_t^\gamma(x_{t-1}; \boldsymbol{\theta}) := \int f(x_{t-1}, x_t; \boldsymbol{\theta}) \gamma_t(x_t) dx_t$ are normalization terms for the probability densities h^γ and f_t^γ , respectively. To ensure that the parameter likelihood estimate $\hat{p}(\mathbf{y} | \boldsymbol{\theta})$ remains unbiased under the twisted model, we define the twisted state-dependent likelihoods $g_1^\gamma, \dots, g_T^\gamma$ as functions that satisfy

$$\begin{aligned} \hat{p}(\mathbf{x}, \mathbf{y} | \boldsymbol{\theta}) &= h^\gamma(x_1) \cdot \prod_{t=2}^T f_t^\gamma(x_{t-1}, x_t; \boldsymbol{\theta}) \cdot \prod_{t=1}^T g_t^\gamma(x_t, y_t; \boldsymbol{\theta}) \\ h(x_1) \cdot \prod_{t=2}^T f(x_{t-1}, x_t; \boldsymbol{\theta}) \cdot \prod_{t=1}^T g(x_t, y_t; \boldsymbol{\theta}) &= \frac{h(x_1) \gamma_1(x_1)}{H^\gamma} \cdot \prod_{t=2}^T \frac{f(x_{t-1}, x_t; \boldsymbol{\theta}) \gamma_t(x_t; \boldsymbol{\theta})}{F_t^\gamma(x_{t-1}; \boldsymbol{\theta})} \cdot \prod_{t=1}^T g_t^\gamma(x_t, y_t; \boldsymbol{\theta}) \\ \prod_{t=1}^T g(x_t, y_t; \boldsymbol{\theta}) &= \frac{\gamma_1(x_1)}{H^\gamma} \cdot \prod_{t=2}^T \frac{\gamma_t(x_t)}{F_t^\gamma(x_{t-1}; \boldsymbol{\theta})} \cdot \prod_{t=1}^T g_t^\gamma(x_t, y_t; \boldsymbol{\theta}) \end{aligned}$$

This equality can be maintained if we define $g_1^\gamma, \dots, g_T^\gamma$ as follows,

$$\begin{aligned} g_1^\gamma(x_1, y_1; \boldsymbol{\theta}) &:= \frac{H^\gamma \cdot g(x_1, y_1; \boldsymbol{\theta}) \cdot F_2^\gamma(x_1; \boldsymbol{\theta})}{\gamma_1(x_1)} \\ g_t^\gamma(x_t, y_t; \boldsymbol{\theta}) &:= \frac{g(x_t, y_t; \boldsymbol{\theta}) \cdot F_{t+1}^\gamma(x_t; \boldsymbol{\theta})}{\gamma_t(x_t)} \quad \text{for all } t = 2, \dots, T-1 \\ g_T^\gamma(x_T, y_T; \boldsymbol{\theta}) &:= \frac{g(x_T, y_T; \boldsymbol{\theta})}{\gamma_T(x_T)} \end{aligned}$$

Thus, the parameter likelihood estimate of the twisted model is

$$\hat{p}^\gamma(\mathbf{y} | \boldsymbol{\theta}) = \prod_{t=1}^T \left(\frac{1}{S} \sum_{s=1}^S g_t^\gamma(x_t^s, y_t; \boldsymbol{\theta}) \right)$$

The BPF is simply a degenerate case of twisted SMC in which $\gamma_t = 1$ for all t .

1.3 Determining the Optimal Policy γ^*

The variance of the estimate \hat{p}^γ comes from the state-dependent likelihood g . Thus, to minimize the variance, we would like g_t^γ to be as uniform as possible with respect to x_t . Let the optimal policy be denoted γ^* . It follows that

$$\begin{aligned} \gamma_T^*(x_T) &:= g(x_T, y_T; \boldsymbol{\theta}) \\ \gamma_t^*(x_t) &:= g(x_t, y_t; \boldsymbol{\theta}) \cdot F_{t+1}^{\gamma^*}(x_t; \boldsymbol{\theta}) \quad \text{for all } t = 1, \dots, T-1 \end{aligned}$$

Under γ^* , the likelihood estimate $\hat{p}^{\gamma^*}(\mathbf{y}|\boldsymbol{\theta}) = H^{\gamma^*} = p(\mathbf{y}|\boldsymbol{\theta})$ has zero variance. However, it may be infeasible for us to use γ^* in many cases, because the BPF algorithm requires us to sample x_t from $f_t^{\gamma^*}$ for all t . For example, under γ^* , we would have

$$f_T^{\gamma^*}(x_{T-1}, x_T; \boldsymbol{\theta}) \propto f(x_{T-1}, x_T; \boldsymbol{\theta}) \cdot \gamma_T^*(x_T) = f(x_{T-1}, x_T; \boldsymbol{\theta}) \cdot g(x_T, y_T; \boldsymbol{\theta})$$

which may be impossible to directly sample from if f and g form an intractable posterior (e.g. if f is Gaussian and g is binomial). Therefore, we must choose a suboptimal policy γ .

1.4 Choosing γ for the Neuroscience Application

Recall the neuroscience model, in which we have

$$\begin{aligned} h(x_1) &= \mathcal{N}(x_1 | x_0, \psi_0) \\ f(x_{t-1}, x_t; \boldsymbol{\theta}) &= \mathcal{N}(x_t | x_{t-1} + \mu_t, \psi) \\ g(x_t, y_t) &= \text{Binomial}\left(R, \frac{\exp x_t}{1 + \exp x_t}\right), \end{aligned}$$

where we define the parameters $\boldsymbol{\theta} = \{\psi, \boldsymbol{\mu}\}$, where $\boldsymbol{\mu} = \{\mu_1, \dots, \mu_T\}$.

Remark: In the main text, we set $\mu_t = 0$ for all $t \neq t_0$ and $\mu_{t_0} = \mu$. This makes the derivation below more general.

Here, we can show that $F_{t+1}^{\gamma^*}(x_t; \boldsymbol{\theta}) := \int f(x_t, x_{t+1}; \boldsymbol{\theta}) \gamma_{t+1}^*(x_{t+1}) dx_{t+1}$ must be log-concave in x_t . This further implies that for all t , $\gamma_t^*(x_t) := g(x_t, y_t) \cdot F_{t+1}^{\gamma^*}(x_t; \boldsymbol{\theta})$ is a log-concave function of x_t since the product of two log-concave functions is log-concave. Hence, we have shown that the optimal policy $\gamma^* = \{\gamma_1^*, \dots, \gamma_T^*\}$ is a series of log-concave functions. This justifies the approximation of each $\gamma_t^*(x_t)$ with a Gaussian function

$$\gamma_t(x_t) = \exp(-a_t x_t^2 - b_t x_t - c_t), \quad (a_t, b_t, c_t) \in \mathbb{R}^3$$

and thus, $f_t^\gamma(x_{t-1}, x_t; \boldsymbol{\theta}) \propto f(x_{t-1}, x_t; \boldsymbol{\theta}) \cdot \gamma_t(x_t)$ is also a Gaussian density that is easy to sample from when running the BPF algorithm.

We want to find the values of (a_t, b_t, c_t) that enforce $\gamma_t \approx \gamma_t^*$ for all t . One simple way to accomplish this goal is to find the (a_t, b_t, c_t) that minimizes the least-squares difference between γ_t and γ_t^* in log-space. That is, given a set of samples $\{x_t^1, \dots, x_t^S\}$ for the random variable x_t , we solve for

$$\begin{aligned} (a_t, b_t, c_t) &= \arg \min_{(a_t, b_t, c_t) \in \mathbb{R}^3} \sum_{s=1}^S [\log \gamma_t(x_t^s) - \log \gamma_t^*(x_t^s)]^2 \\ &= \arg \min_{(a_t, b_t, c_t) \in \mathbb{R}^3} \sum_{s=1}^S [-(a_t(x_t^s)^2 + b_t(x_t^s) + c_t) - \log \gamma_t^*(x_t^s)]^2 \end{aligned}$$

Also note that in a slight abuse of notation, we redefine for all $t < T$,

$$\gamma_t^*(x_t) := g(x_t, y_t) \cdot F_{t+1}^\gamma(x_t; \boldsymbol{\theta}_t)$$

because when performing approximate backwards recursion, it is not possible to analytically solve for the intractable integral $F_{t+1}^{\gamma^*}(x_t; \boldsymbol{\theta}_t)$.

In the aforementioned least-squares optimization problem, there is one additional constraint that we must take into account. Recall that $f_t^\gamma(x_{t-1}, x_t; \boldsymbol{\theta}) \propto f(x_{t-1}, x_t; \boldsymbol{\theta}) \cdot \gamma_t(x_t)$ is a Gaussian pdf that we sample from. Therefore, we must ensure that the variance of this distribution is positive, which places a constraint on γ_t and more specifically, the domain of (a_t, b_t, c_t) . Using properties of Gaussians, we can perform algebraic manipulation to work out the following parameterizations of h^γ and f_t^γ :

$$\begin{aligned} h^\gamma(x_1) &= \mathcal{N}\left(x_1 \mid \frac{\psi_0^{-1} \cdot (x_0 + \mu_1) - b_1}{\psi_0^{-1} + 2a_1}, \frac{1}{\psi_0^{-1} + 2a_1}\right) \\ f_t^\gamma(x_{t-1}, x_t; \boldsymbol{\theta}) &= \mathcal{N}\left(x_t \mid \frac{\psi^{-1} \cdot (x_{t-1} + \mu_t) - b_t}{\psi^{-1} + 2a_t}, \frac{1}{\psi^{-1} + 2a_t}\right) \quad \text{for all } t = 2, \dots, T \end{aligned}$$

The corresponding normalizing terms for these densities are

$$H^\gamma = \frac{1}{\sqrt{1+2a_1\psi_0}} \exp\left(\frac{\psi_0^{-1} \cdot (x_0 + \mu_1) - (b_1)^2}{2(\psi_0^{-1} + 2a_1)} - \frac{(x_0 + \mu_1)^2}{2\psi_0} - c_1\right)$$

$$F_t^{\gamma'}(x_{t-1}; \boldsymbol{\theta}) = \frac{1}{\sqrt{1+2a_t\psi}} \exp\left(\frac{\psi^{-1} \cdot (x_{t-1} + \mu_t) - (b_t)^2}{2(\psi^{-1} + 2a_t)} - \frac{(x_{t-1} + \mu_t)^2}{2\psi} - c_t\right) \quad \text{for all } t = 2, \dots, T$$

Thus, to obtain (a_t, b_t, c_t) and consequently γ_t for all t , we solve the aforementioned least-squares minimization problem subject to the following constraints:

$$a_1 > -\frac{1}{2\psi_0} \qquad a_t > -\frac{1}{2\psi} \quad \text{for all } t = 2, \dots, T$$

1.4.1 Full cSMC Algorithm

The full controlled sequential Monte Carlo algorithm iterates on twisted SMC for L iterations, building a series of policies $\gamma^{(1)}, \gamma^{(2)}, \dots, \gamma^{(L)}$ over time. Given two policies Γ' and γ , we can define

$$h^{\Gamma' \cdot \gamma}(x_1) \propto h^{\Gamma'}(x_1) \gamma_1(x_1) = h(x_1) \cdot \Gamma'_1(x_1) \cdot \gamma_1(x_1)$$

$$f_t^{\Gamma' \cdot \gamma}(x_{t-1}, x_t; \boldsymbol{\theta}) \propto f_t^{\Gamma'}(x_{t-1}, x_t; \boldsymbol{\theta}) \cdot \gamma_t(x_t) = f(x_{t-1}, x_t; \boldsymbol{\theta}) \cdot \Gamma'_t(x_t) \cdot \gamma_t(x_t)$$

We can see from these relationships that twisting the original model using Γ' and then twisting the new model using γ has the same effect as twisting the original model using a cumulative policy Γ where each $\Gamma_t(x_t) = \Gamma'_t(x_t) \cdot \gamma_t(x_t)$.

We state the full cSMC algorithm in Algorithm 3.

Algorithm 3 ControlledSMC($\mathbf{y}, g, \psi, x_0, \psi_0, \boldsymbol{\mu}, L$)

- 1: Define $f(x_{t-1}, x_t; \boldsymbol{\theta}) := \mathcal{N}(x_t | x_{t-1} + \mu_t, \psi)$ and $h(x_1) := \mathcal{N}(x_1 | x_0 + \mu_1, \psi_0)$.
 - 2: Define parameters $\boldsymbol{\theta} = \{\psi, \boldsymbol{\mu}\}$.
 - 3: Collect particles $\{x_1^s\}_{s=1}^S, \dots, \{x_T^s\}_{s=1}^S$ from `BootstrapParticleFilter`($\mathbf{y}, \boldsymbol{\theta}, f, g, h$).
 - 4: Initialize $\Gamma' = \{\Gamma'_1, \dots, \Gamma'_T\}$ where $\Gamma'_t(x_t) = 1$ for all $t = 1, \dots, T$.
 - 5: Initialize $g_t^{\Gamma'}(x_t, y_t) = g(x_t, y_t)$ for all $t = 1, \dots, T$.
 - 6: Initialize $a_t^{(0)} = 0, b_t^{(0)} = 0, c_t^{(0)} = 0$ for all $t = 1, \dots, T$.
-

Algorithm 4 ControlledSMC (*continued*)

```
7: for  $\ell = 1, \dots, L$  do
  // Approximate backward recursion to determine policy and associated functions
8:   Define  $\gamma_T^*(x_T) := g_T^{\Gamma'}(x_T, y_T)$ .
9:   for  $t = T, \dots, 2$  do
10:    Solve  $(a_t^{(\ell)}, b_t^{(\ell)}, c_t^{(\ell)}) = \arg \min_{(a_t, b_t, c_t)} \sum_{s=1}^S [-(a_t(x_t^s)^2 + b_t(x_t^s) + c_t) - \log \gamma_t^*(x_t^s)]^2$  subject to
     $a_t > -1/(2\psi) - \sum_{\ell'=0}^{\ell-1} a_t^{(\ell')}$  using linear regression.
11:    Define new policy function  $\gamma_t(x_t) := \exp(-a_t^{(\ell)} x_t^2 - b_t^{(\ell)} x_t - c_t^{(\ell)})$ .
12:    Define cumulative policy function  $\Gamma_t(x_t) := \Gamma_t^{\Gamma'}(x_t) \cdot \gamma_t(x_t) = \exp(-A_t x_t^2 - B_t x_t - C_t)$  where
     $A_t := \sum_{\ell'=0}^{\ell} a_t^{(\ell')}$ ,  $B_t := \sum_{\ell'=0}^{\ell} b_t^{(\ell')}$ , and  $C_t := \sum_{\ell'=0}^{\ell} c_t^{(\ell')}$ .
13:    Define  $f_t^{\Gamma}(x_{t-1}, x_t; \theta)$  and  $F_t^{\Gamma}(x_{t-1}; \theta)$ .
14:    if  $t = T$  then
15:      Define  $g_T^{\Gamma}(x_T, y_T) := \frac{g(x_T, y_T)}{\Gamma_T(x_T)}$ .
16:    else
17:      Define  $g_t^{\Gamma}(x_t, y_t) := \frac{g(x_t, y_t) \cdot F_{t+1}^{\Gamma}(x_t; \theta)}{\Gamma_t(x_t)}$ .
18:    end if
19:    Define  $\gamma_{t-1}^*(x_{t-1}) := g_{t-1}^{\Gamma'}(x_{t-1}, y_{t-1}) \cdot F_t^{\Gamma}(x_{t-1}; \theta) / F_t^{\Gamma'}(x_{t-1}; \theta)$ .
20:  end for
21:  Solve  $(a_1^{(\ell)}, b_1^{(\ell)}, c_1^{(\ell)}) = \arg \min_{(a_1, b_1, c_1)} \sum_{s=1}^S [-(a_1(x_1^s)^2 + b_1(x_1^s) + c_1) - \log \gamma_1^*(x_1^s)]^2$  subject to
   $a_1 > -1/(2\psi_0) - \sum_{\ell'=0}^{\ell-1} a_1^{(\ell')}$  using linear regression.
22:  Define new policy function  $\gamma_1(x_1) := \exp(-a_1^{(\ell)} x_1^2 - b_1^{(\ell)} x_1 - c_1^{(\ell)})$ .
23:  Define cumulative policy function  $\Gamma_1(x_1) := \Gamma_1^{\Gamma'}(x_1) \cdot \gamma_1(x_1) = \exp(-A_1 x_1^2 - B_1 x_1 - C_1)$  where  $A_1 :=$ 
   $\sum_{\ell'=0}^{\ell} a_1^{(\ell')}$ ,  $B_1 := \sum_{\ell'=0}^{\ell} b_1^{(\ell')}$ , and  $C_1 := \sum_{\ell'=0}^{\ell} c_1^{(\ell')}$ .
24:  Define  $\Gamma$ -twisted initial prior  $h^{\Gamma}(x_1)$  and  $H^{\Gamma}$ .
25:  Define  $g_1^{\Gamma}(x_1, y_1) := \frac{H^{\Gamma} \cdot g(x_1, y_1) \cdot F_2^{\Gamma}(x_1; \theta)}{\Gamma_1(x_1)}$ .
  // Forward bootstrap particle filter to sample particles and compute weights
26:  for  $s = 1, \dots, S$  do
27:    Sample  $x_1^s \sim h^{\Gamma}(x_1)$ .
28:    Weight  $w_1^s = g_1^{\Gamma}(x_1^s, y_1)$ .
29:  end for
30:  Normalize  $\{w_1^s\}_{s=1}^S = \{w_1^s\}_{s=1}^S / \sum_{s=1}^S w_1^s$ .
31:  for  $t = 2, \dots, T$  do
32:    for  $s = 1, \dots, S$  do
33:      Resample ancestor index  $a \sim \text{Categorical}(w_{t-1}^1, \dots, w_{t-1}^S)$ .
34:      Sample  $x_t^s \sim f_t^{\Gamma}(x_{t-1}^a, x_t; \theta)$ .
35:      Weight  $w_t^s = g_t^{\Gamma}(x_t^s, y_t)$ .
36:    end for
37:    Normalize  $\{w_t^s\}_{s=1}^S = \{w_t^s\}_{s=1}^S / \sum_{s=1}^S w_t^s$ .
38:  end for
39:  Update  $\Gamma' \leftarrow \Gamma$ .
40: end for
41: return Likelihood estimate  $\hat{p}^{\Gamma}(y | \theta)$ .
```

2 Clustering Cue Responses: Figures of Additional Clusters

Following cluster selection, we identified a total of 9 different types of responses to the cue. The overlaid rasters from two of these clusters are shown in Figure 4. Figures 8-14 shows the additional clusters. Together, Figure 4 and 8-14 demonstrate the ability of our approach to cluster neural responses to a stimulus into a set of clusters whose overlaid rasters are not unlike typical responses from single neurons.

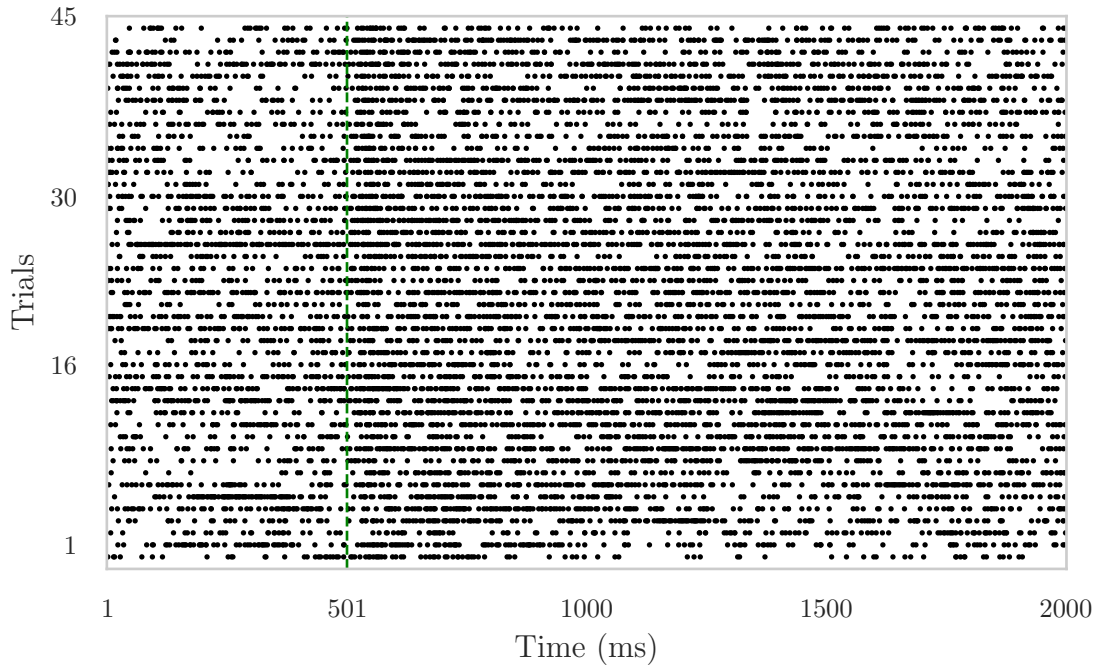


Figure 8: Overlaid raster plots of neurons with very excited and unsustained responses. A black dot indicates a spike from at least one of the neurons in the corresponding cluster. The vertical green line indicates cue onset.

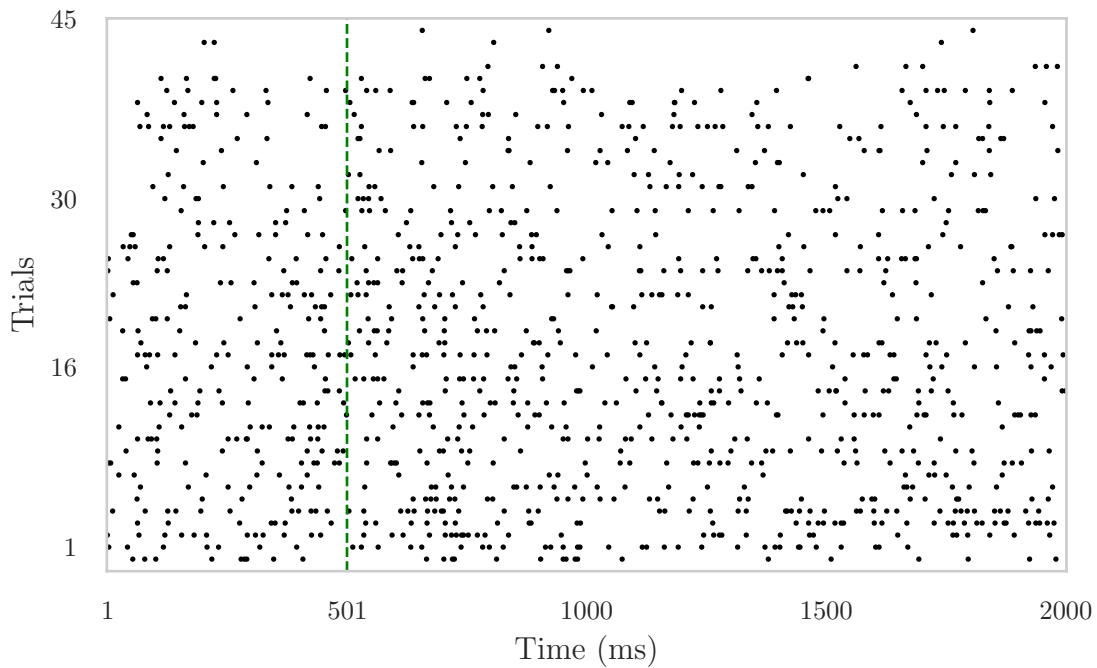


Figure 9: Overlaid raster plots of neurons with moderately excited and unsustained responses. A black dot indicates a spike from at least one of the neurons in the corresponding cluster. The vertical green line indicates cue onset.

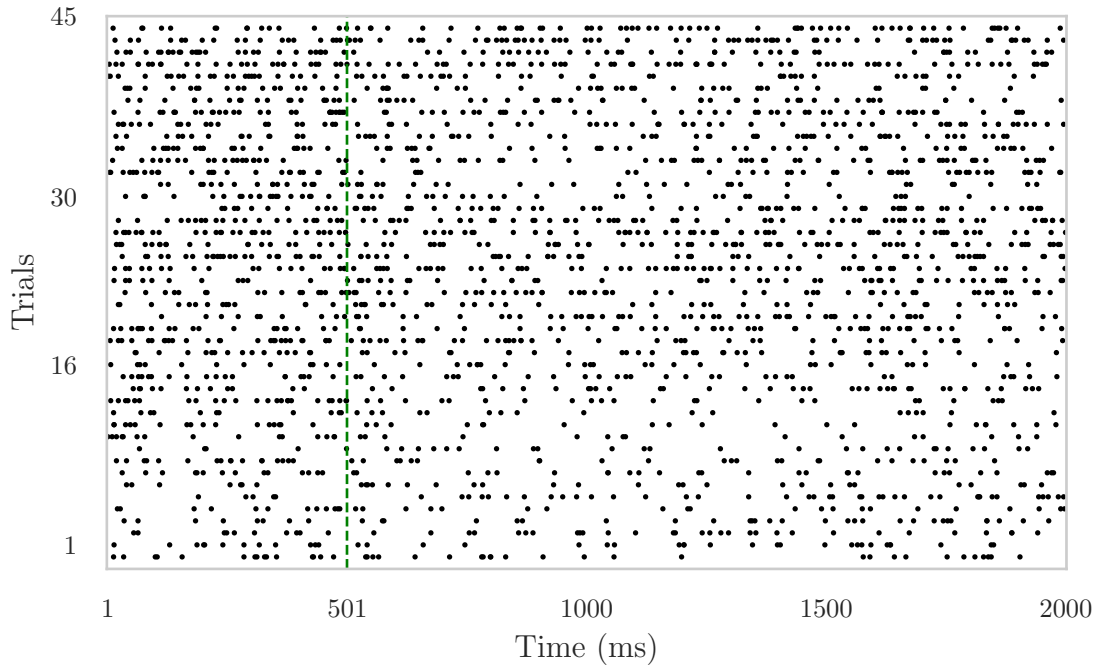


Figure 10: Overlaid raster plots of neurons with very inhibited and unsustained responses. A black dot indicates a spike from at least one of the neurons in the corresponding cluster. The vertical green line indicates cue onset.

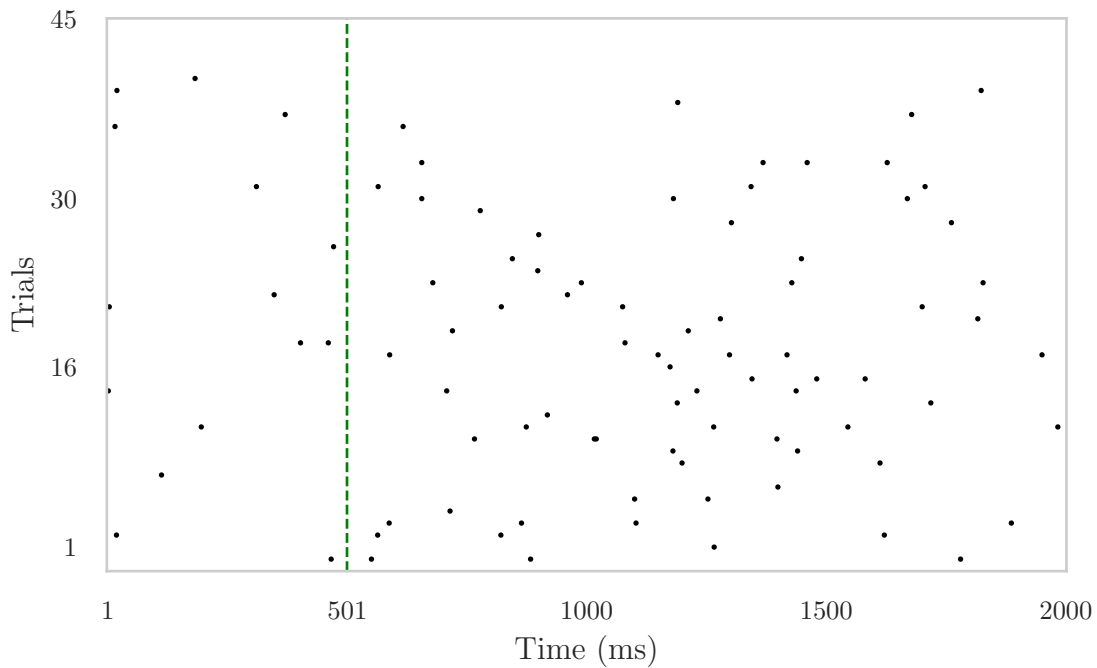


Figure 11: Overlaid raster plots of neurons with moderately excited and sustained responses. A black dot indicates a spike from at least one of the neurons in the corresponding cluster. The vertical green line indicates cue onset.

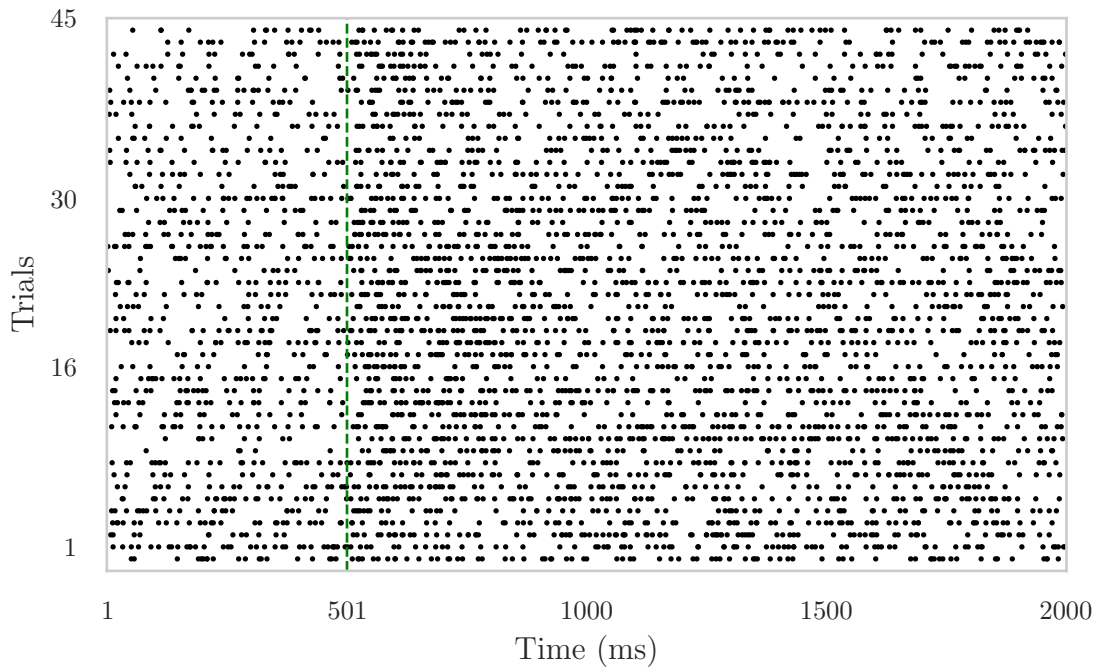


Figure 12: Overlaid raster plots of neurons with very excited and unsustained responses. A black dot indicates a spike from at least one of the neurons in the corresponding cluster. The vertical green line indicates cue onset.

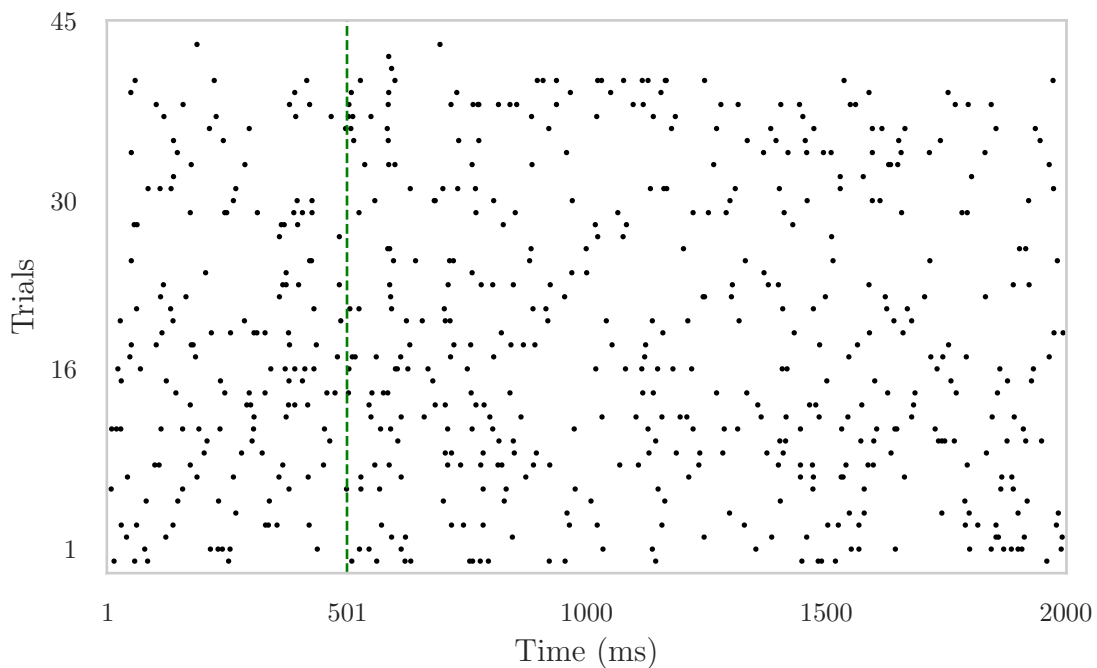


Figure 13: Overlaid raster plots of neurons with slightly inhibited and sustained responses. A black dot indicates a spike from at least one of the neurons in the corresponding cluster. The vertical green line indicates cue onset.

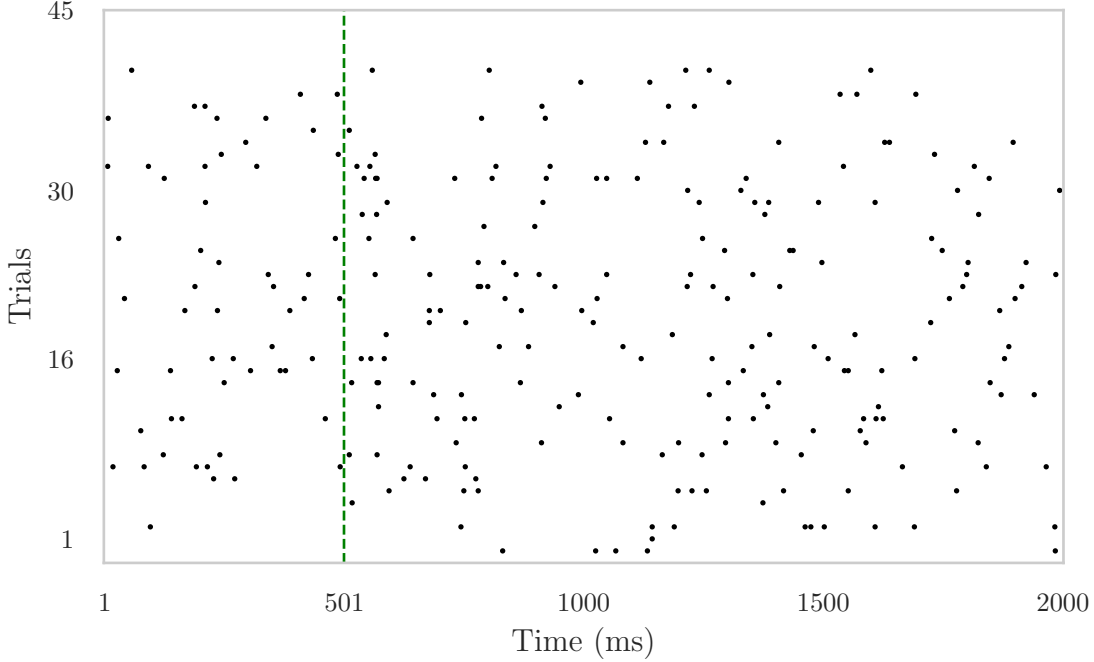


Figure 14: Overlaid raster plots of neurons with slightly excited and sustained responses. A black dot indicates a spike from at least one of the neurons in the corresponding cluster. The vertical green line indicates cue onset.

3 Clustering Shock Responses: How subtle is the effect Figure 6(b) (main text)?

The fact that Figure 6(b) comprises neurons that are inhibited in response to the shock is not visually apparent. We pick two neurons from the cluster and demonstrate that the shock has an inhibitory, albeit subtle, effect on their response. In particular, we compare the empirical estimate of the rate at all trials $1, \dots, 45$ to an estimate of the rate obtained from the DPnSSM model.

We compute the empirical rate of events at trial t in units of Hz as $\hat{\lambda}_t^{\text{emp}} = 1000 \cdot y_t^{(n)} / 2000$, where the factor of 1000 is to convert the empirical probability estimates to units of Hz.

Suppose the cluster selection method described in the main text selects the samples from Gibbs iteration i^* . For a given neuron n with cluster assignment $z^{(n)(i^*)}$ and parameter $\theta^{(z^{(n)(i^*)})}$ obtained from hierarchical clustering applied to the co-occurrence matrix (please see main text), we use cSMC to generate $S = 64$ samples x_1^s, \dots, x_T^s , where for each $t = 1, \dots, T$,

$$x_t^s \sim p(x_t^{(n)} | z^{(n)(i^*)}, \theta^{(z^{(n)(i^*)})}, y_1^{(n)}, \dots, y_t^{(n)}) \quad (1)$$

for all s . We then compute

$$\hat{x}_t = \frac{1}{S} \sum_{s=1}^S x_t^s. \quad (2)$$

Finally, as the DPnSSM estimate of the rate in Hz, we use

$$\hat{\lambda}_t^{\text{dpnssm}} = 1000 \left(\frac{\exp \hat{x}_t}{1 + \exp \hat{x}_t} \right) \quad (3)$$

Figure 15 shows two neurons from the cluster in Figure 6(b). Overall, the empirical rate from each neuron indicates a downward trend, that is accentuated around trial 16, the trial when shock is delivered. In the DPnSSM, this is captured by the abrupt change in the empirical rate at trial 16, which indicates the fact that these neurons are inhibited, albeit very subtly so, in response to the shock. In other words, despite the fact this effect is not obvious from the overlaid raster of Figure 6(b), Figure 15 indicates that the DPnSSM is able to identify a subtle effect that can be seen in the raw data.

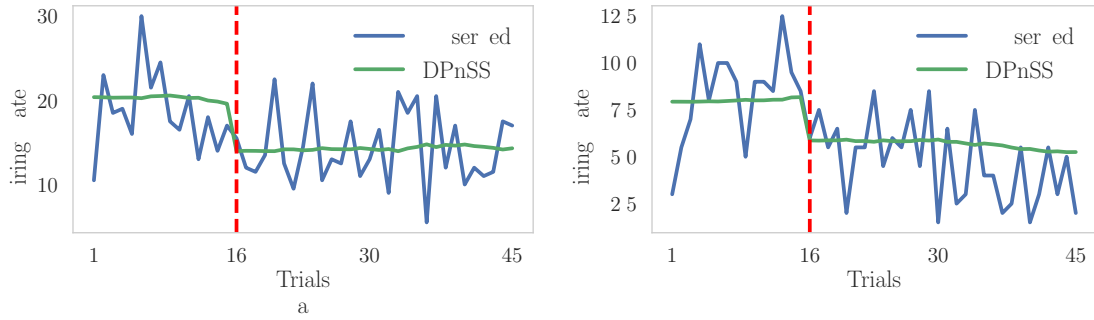


Figure 15: Two representative neurons from the cluster corresponding to Figure 6(b). The DPnSSM state sequence is able to track the overall trend in the observed data and correctly characterize the response to the shock at trial 16 as slightly inhibited.

References

- Pieralberto Guarniero, Adam M Johansen, and Anthony Lee. The iterated auxiliary particle filter. *Journal of the American Statistical Association*, 112(520):1636–1647, 2017.
- Jeremy Heng, Adrian N Bishop, George Deligiannidis, and Arnaud Doucet. Controlled Sequential Monte Carlo. *arXiv preprint arXiv:1708.08396*, 2017.